MATERIALS CHEMISTRY FRONTIERS

RESEARCH ARTICLE

View Article Online
View Journal | View Issue

Cite this: *Mater. Chem. Front.*, 2026, **10**, 245

Orange-red RTP co-crystals with acid/base-triggered responsive phosphorescence

Yuxuan Song, Xingjia Jiang, Guocui Pan, Bin Xu * and Wenjing Tian *

Received 30th September 2025,
Accepted 21st November 2025

DOI: 10.1039/d5qm00717h

rsc.li/frontiers-materials

In recent years, co-crystallization has emerged as an effective approach to designing room-temperature phosphorescent (RTP) materials. However, achieving long-wavelength-emissive RTP remains challenging, due to the non-radiative deactivation, which arises from the inherently small energy gap between the lowest excited triplet state (T_1) and the ground state (S_0). In this study, we constructed two orange-red RTP co-crystals based on 2,4′-bipyridine (24BD) and 1,4-diiodotetrafluorobenzene (DITF) or 1,3,5-trifluoro-2,4,6-triiodobenzene (TITF). The co-crystals exhibit distinct phosphorescence properties with main emission peaks at 570 nm, with lifetimes of 32.69 ms and 22.10 ms, respectively. Crystal structure analysis and theoretical calculations indicated that tight π–π stacking and abundant intermolecular interactions within the co-crystals are responsible for the long-wavelength RTP. Interestingly, the two co-crystals exhibit distinct acid–base stimulus-responsive properties. The phosphorescence of the 24BD-DITF crystals was quenched after acid fumigation, but recovered after subsequent alkali fumigation, owing to the cleavage and reformation of halogen bonds. In contrast, the phosphorescence of the 24BD-TITF co-crystal was quenched by acid treatment and could not be restored by alkali fumigation due to its weak halogen bond, instead showing orange fluorescence. This study introduces a new material system for achieving long-wavelength RTP in organic co-crystals, and provides a foundation for developing acid–base stimulus-responsive materials for future applications.

Introduction

RTP of purely organic compounds has attracted significant attention because of its long lifetime, low cost, and unique responsiveness to external stimuli, which is attributed to a large Stokes shift and the sensitivity of triplet excitons to the surrounding environment.[1–9] Currently, strategies to achieve RTP focus on enhancing the generation of triplet excitons through the incorporation of functional groups, including heteroatoms,[10–14] heavy atoms,[15–17] or lone pairs of electrons (such as C=O, C=S, NR_2, *etc.*)[18,19] and suppressing non-radiative deactivation of triplet states *via* strategies like crystallization,[20–26] host–guest doping,[27–30] metal–organic frameworks (MOFs),[31–33] ionic bonding,[34,35] polymer embedding,[36–38] and supramolecular self-assembly.[39–41]

Among these, co-crystal engineering represents an effective approach to achieve RTP. The formation of co-crystals by combining host and guest molecules enhances structural rigidity and prevents self-quenching of the phosphors, thus enhancing RTP emission.[42–47] Additionally, the new intermolecular interactions formed during co-crystallization provide additional stability. Furthermore, the clear and regular structure of co-crystals facilitates the investigation of the relationship between the aggregation structure and RTP properties. In recent years, several studies have utilized co-crystal engineering to achieve RTP emission. For example, Huang and co-workers employed supramolecular self-assembly of melamine and isophthalic acid to form a co-crystal.[48] Multiple intermolecular interactions within the rigid MA-IPA supramolecular framework effectively reduced non-radiative deactivation and finally promoted the generation of green RTP in the co-crystal. Similarly, Shi and co-workers developed a series of co-crystals from melamine and carboxylic acids with varying alkyl chain lengths.[49] These co-crystals exhibited blue RTP, with lifetimes increasing as the alkyl chain length was manipulated. Recently, Ren and co-workers created a family of chiral co-crystals by aromatic carboxylic acids and R/S-THNA.[50] Due to the rigidity, chirality and isolated environment provided by the cocrystallization of the components, the co-crystals exhibited blue and cyan RTP, as well as circularly polarized persistent phosphorescence and large second harmonic generation properties. However, due to nonradiative deactivation from the inherent small energy gap between the lowest excited triplet state (T_1) and the ground state (S_0), it remains a significant challenge to achieve long-wavelength RTP in co-crystals.

State Key Laboratory of Supramolecular Structure and Materials, College of Chemistry, Jilin University, Changchun, 130012, P. R. China.
E-mail: xubin@jlu.edu.cn

Herein, we successfully constructed two orange-red RTP co-crystals by introducing halogen bonds and π–π interactions, designated as 24BD-DITF and 24BD-TITF. The two co-crystals demonstrate different acid–base stimulus-responsive properties. After acid fumigation, both co-crystals show phosphorescence quenching. However, following subsequent alkaline fumigation, the RTP of 24BD-DITF was restored, attributable to its strong halogen bonds, whereas that of 24BD-TITF remains quenched due to weaker halogen bonds. This study not only provides new insights into stimulus-responsive organic luminescent materials, but also offers a novel strategy for further designing long-wavelength RTP materials.

Results and discussion

We selected 2,4′- bipyridine (24BD) as the host molecule, and 1,4-diiodotetrafluorobenzene (DITF) along with 1,3,5-trifluoro-2,4,6-triiodobenzene (TITF) as the guest molecules to prepare 24BD-DITF and 24BD-TITF co-crystals *via* a solvent evaporation method (Fig. 1a). Under 365 nm UV excitation, pure 24BD powder exhibited a fluorescence emission peak at 521 nm, with a lifetime of 2.34 ns. And the host molecule 24BD also didn't exhibit phosphorescence emission in solution and crystalline states (Fig. S1–S3). After introducing the guest molecules, the luminescent properties of the co-crystals differed significantly from those of pure 24BD powder. Both co-crystals exhibited a blue-shift in the main fluorescence peaks to 445 nm, showing blue fluorescence (Fig. 1b and c). The fluorescence lifetime and quantum yield of the 24BD-DITF co-crystal were 2.47 ns and 6.32%, while those of the 24BD-TITF co-crystal were 1.73 ns and 0.06%, respectively (Fig. S8). Additionally, the absorption spectra of the co-crystals displayed broad absorption ranges, with some weak absorption peaks and a trailing edge extending to approximately 700 nm (Fig. S11). These results indicate that the introduction of guest molecules will create effective conjugated structures that facilitate long-wavelength emission, and further increase the richness of the band, making RTP emission possible in these co-crystals.

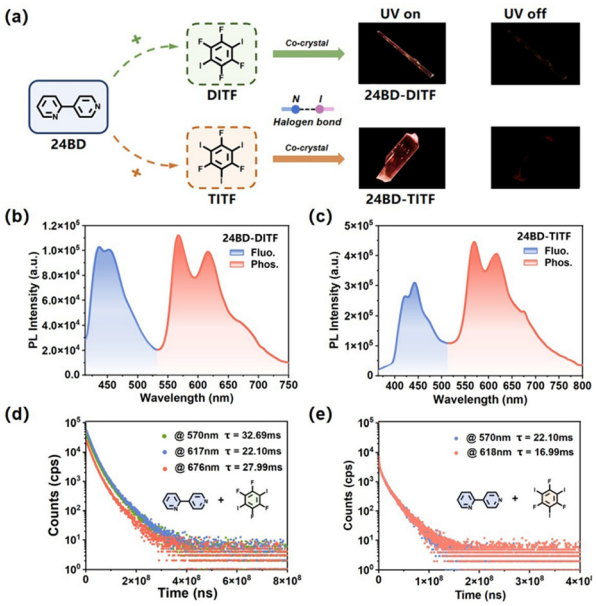

Fig. 1 (a) Molecular structure of 24BD, DITF, TITF and the fluorescence microscope photographs of 24BD-DITF and 24BD-TITF co-crystals under UV light (365 nm). PL spectra of (b) 24BD-DITF and (c) 24BD-TITF co-crystals. λ_{ex} = 365 nm. Phosphorescence lifetime of (d) 24BD-DITF and (e) 24BD-TITF co-crystals.

After UV irradiation ceased, the co-crystals showed an orange-red afterglow. The phosphorescence of 24BD was effectively activated by the exogenous heavy atom effect. The phosphorescence emission peaks of the 24BD-DITF co-crystal were observed at 570 nm, 617 nm and 676 nm, with corresponding lifetimes of 32.69 ms, 27.05 ms and 27.99 ms, respectively (Fig. 1d). The phosphorescence quantum yield (Φ_{Ph}) of the crystal reached as high as 9.63%. In contrast, the 24BD-TITF co-crystal exhibited two phosphorescence peaks at 570 nm and 617 nm, with lifetimes of 22.10 ms and 16.99 ms, and Φ_{Ph} of 0.09% (Fig. 1e). The RTP properties of both co-crystals were further confirmed by temperature-dependent and time-resolved spectroscopy (Fig. S14 and S15). Furthermore, the photophysical parameters of the 24BD-DITF and 24BD-TITF co-crystals were calculated. As shown in Table S1, for the 24BD-DITF crystal, the phosphorescence rate (k_{ph}) is 3.14 s^{-1}, while the triplet non-radiative decay rate ($k_{Ph,nr}$) is 27.45 s^{-1}, approximately 8.7 times higher than k_{ph}. In contrast, for the 24BD-TITF crystal, its k_{ph} is 0.055 s^{-1}, and the $k_{Ph,nr}$ is 60.88 s^{-1}, about 1106 times higher than k_{ph}. Therefore, compared to 24BD-TITF, 24BD-DITF shows more efficient radiative decay pathways, resulting in a relatively high Φ_{Ph}.

To further investigate the relationship between RTP properties and aggregation structure, the crystal structures and intermolecular interactions of the two co-crystals were analyzed. As shown in Fig. 2a and b, 24BD-DITF and 24BD-TITF are packed in a separated column mode in the single crystal unit cell. The stoichiometric ratio of 24BD to DITF is 1 : 2, while that of 24BD to TITF is 1 : 1. Specific parameters of key intermolecular interactions are provided in Tables S3 and S4. The molecular packing structures and main interactions within the co-crystals were further studied. In 24BD-DITF, diverse intermolecular interactions facilitate the formation of a unique aggregated structure. The main interactions are summarized in Fig. 2c and d, including a C–I···N halogen bond with a distance of 2.818 Å and the angle of 174.56°, as well as a C–H···F hydrogen bond with a distance of 2.596 Å and an angle of 133.23°. Besides, 24BD and DITF molecules are arranged in a segregated column along the *b*-axis (Fig. 2i).

In 24BD-TITF co-crystals, each 24BD molecule is connected to the adjacent TITF molecule by a C–I···N halogen bond (distance: 2.934 Å, angle: 167.65°) and C–H···F hydrogen bond (distance: 2.637 Å, angle: 143.36°), resulting in a more compact molecular packing (Fig. 2e and f). Moreover, the molecules are arranged in a segregated column along the *a*-axis (Fig. 2j). Meanwhile, π–π stacking interactions are observed in both co-crystals, contributing significantly to the orange-red RTP emission (Fig. 2g and h).

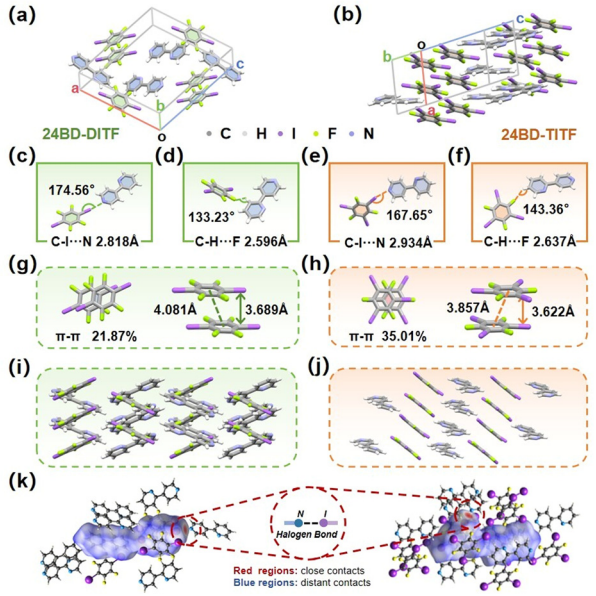

Fig. 2 Single-unit cell structure of the (a) 24BD-DITF and (b) 24BD-TITF co-crystal. Typical hydrogen and halogen bond interactions in the (c) and (d) 24BD-DITF and (e) and (f) 24BD-TITF co-crystal. (g) and (h) π–π stacking interactions of the 24BD-DITF and 24BD-TITF co-crystal. (i) and (j) Stacking modes of the 24BD-DITF and 24BD-TITF co-crystal. (k) Hirshfeld surface analysis of intermolecular interactions in the 24BD-DITF and 24BD-TITF co-crystal.

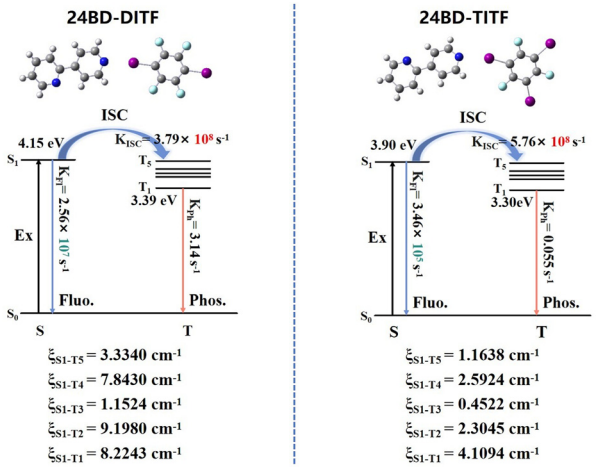

Fig. 3 Theoretically calculated energy levels and spin–orbit coupling constant of the 24BD-DITF and 24BD-TITF co-crystals.

Compared to the 24BD-DITF co-crystals, the halogen bond (C–I···N) in the 24BD-TITF co-crystals exhibits a longer bond length and a smaller bond angle, suggesting a weaker halogen bond. Conversely, 24BD-DITF features stronger π–π stacking and more intermolecular interactions, which is conducive to restricting molecular motion and suppressing non-radiative decay of triplet excitons, corresponding to the higher phosphorescence quantum yield. Hirshfeld surface analysis was conducted using Crystal Explorer to further visualize intermolecular interactions. As shown in Fig. 2i, red dots represent strong intermolecular interactions. In 24BD-DITF, the red dots in the crystal correspond to C–I···N halogen bonds, whereas in 24BD-TITF, both C–I···N and C–H···F interactions are observed. The halogen bond serves as the principal for co-crystal formation and plays a critical role in RTP emission.

Furthermore, based on the molecular structures of the co-crystals, the excited-state properties of the two co-crystals were investigated using time-dependent density functional theory (TD-DFT) from a quantum chemical perspective. To further explore the mechanism underlying their RTP behavior, vertical excitation energies in both the ground and excited states, as well as the spin–orbit coupling (SOC) constants (ξ) between various excited states were calculated (Fig. 3). Typically, efficient intersystem crossing (ISC) requires a singlet–triplet energy gap (ΔE_{ST}) of less than 0.3 eV. Therefore, a detailed excited-state analysis of the co-crystals reveals that there are small ΔE_{ST} values, combined with substantial SOC constants, which facilitate effective transitions from singlet to triplet states. According to Kasha's rule, excited electrons will relax from high energy triplet states to the lowest triplet state (T_1) through an internal conversion process, and finally achieve orange-red RTP in the form of radiation luminescence. Notably, the 24BD-DITF co-crystal exhibits a larger SOC constant than the 24BD-TITF co-crystal, indicating stronger spin–orbit coupling ability, as well as closer energy levels between S_1 and T_5, which is more conducive to promoting the ISC process and RTP emission, thus showing a higher Φ_{Ph}.

The RTP responsive properties of the 24BD-DITF and 24BD-TITF co-crystals under hydrochloric acid (HCl) and triethylamine (TEA) fumigation were further studied (Fig. 4a). Upon exposure to HCl vapor, the 24BD-DITF co-crystals performed significant phosphorescence quenching (Fig. 4b), accompanied by a broad fluorescence peak without a fine structure, and a significant reduction in lifetime to 4.51 ns (Fig. 4c). Interestingly, subsequent TEA fumigation partially restored both fluorescence and phosphorescence. After TEA fumigation, the phosphorescence peak position remained nearly unchanged compared to the original crystals, although the intensity was markedly reduced. Meanwhile, the lifetime of the phosphorescence at 570 nm slightly decreased to 18.17 ms. The same HCl/TEA fumigation was applied to the 24BD-TITF crystal. Following HCl fumigation, both fluorescence and phosphorescence were quenched (Fig. 4e). However, different from the 24BD-DITF crystal, subsequent TEA fumigation resulted in the emergence of orange fluorescence but failed to recover phosphorescence, with the fluorescence lifetime reduced to 3.02 ns (Fig. 4f).

In order to explore the mechanism behind the phosphorescence changes of the co-crystals under acid–base stimulation, wide-angle X-ray diffraction (XRD) analyses were conducted on the co-crystals in their pristine state, after HCl fumigation and after TEA fumigation. As shown in Fig. 4d and g, both 24BD-DITF and 24BD-TITF exhibited significantly weakened diffraction peak intensities after HCl/TEA exposure, indicating reduced crystallinity. As a result, the luminescent intensity of the co-crystals could not fully recover to their original levels.

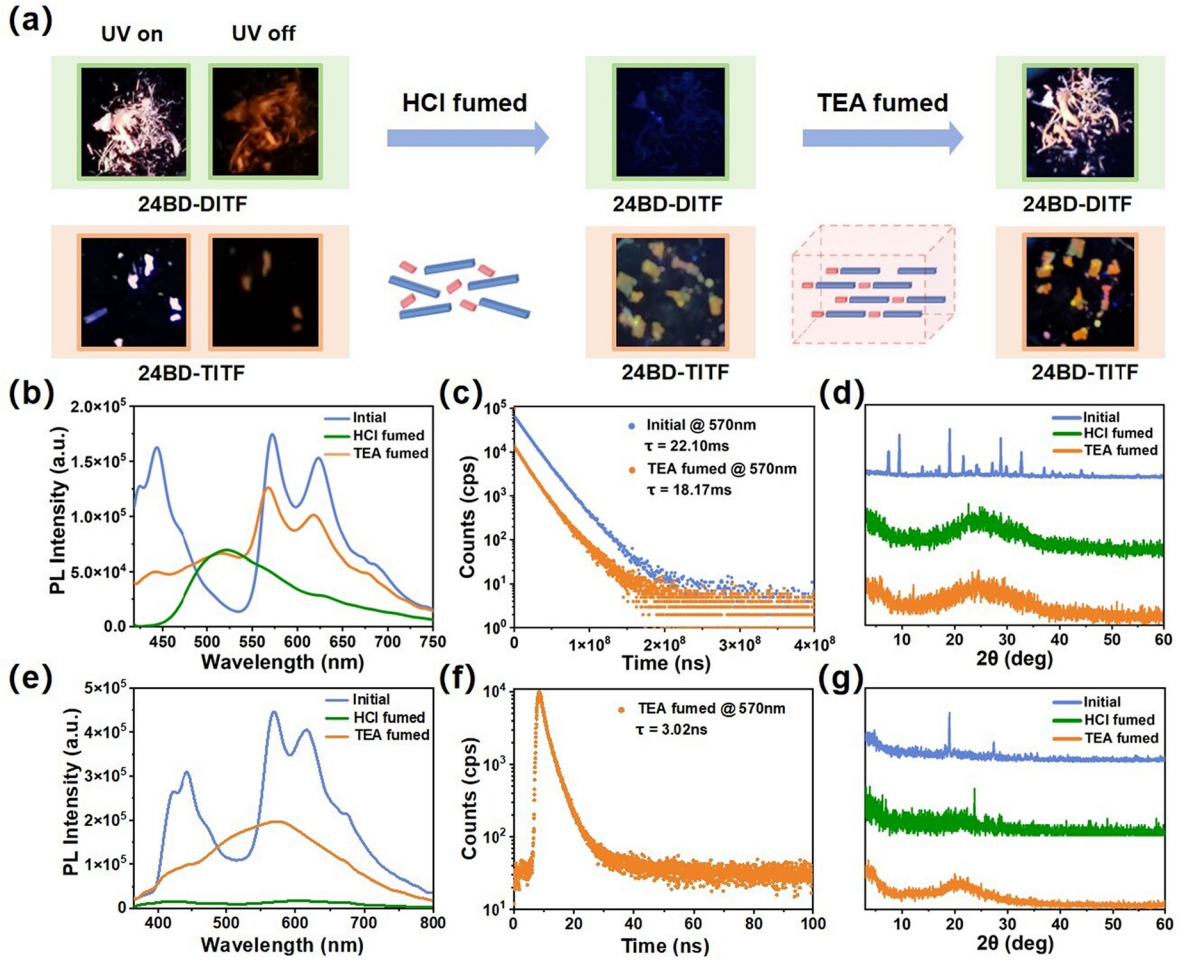

Fig. 4 (a) Images of the 24BD-DITF and 24BD-TITF co-crystals under illumination with 365 nm UV light before and after HCl/TEA treatment. (b) PL spectra of the 24BD-DITF co-crystal before and after HCl/TEA treatment. λ_{ex} = 365 nm. (c) Phosphorescence lifetime of the 24BD-DITF co-crystal at 570 nm before and after HCl/TEA treatment. (d) XRD patterns of 24BD-DITF before and after HCl/TEA treatment. (e) PL spectra of the 24BD-TITF co-crystal before and after HCl/TEA treatment. λ_{ex} = 365 nm. (f) Phosphorescence lifetime of the 24BD-TITF co-crystal at 570 nm after HCl/TEA treatment. (g) XRD patterns of 24BD-TITF before and after HCl/TEA treatment.

Additionally, noticeable shifts in diffraction peak positions suggest changes in the molecular packing mode, which in turn altered the luminescent properties of the materials.

The distinct stimulus-responsive behaviors of the two co-crystals can be attributed to differences in their intermolecular interactions. In the 24BD-DITF crystal, HCl fumigation protonates the pyridyl nitrogen atoms of 24BD. The protonated 24BD molecules dissociate from DITF molecules, which breaks the halogen bonds in the crystal structure and compromises the ISC process, which leads to phosphorescence quenching. At the same time, disruption of the crystal structure and the changing of the aggregation structure results in a change of luminescence properties. For the 24BD-DITF co-crystal, a new emission peak appeared at 520 nm in the PL spectrum. After that, triethylamine can capture the protons and release the neutral pyridine groups, which recombines halogen bonds in the co-crystals, leading to phosphorescence recovery. However, the halogen bonds of the 24BD-TITF co-crystal are relatively weaker, while the binding ability between the nitrogen atom and the proton is stronger. As a result, deprotonation by TEA is less efficient, and the halogen bonds are not easily re-established, ultimately preventing phosphorescence recovery. Moreover, in the 24BD-DITF co-crystal, the proton was only partially removed, and the emission peak at 520 nm appeared after acid treatment was retained.

Conclusions

In summary, two organic orange-red RTP co-crystals were successfully prepared by introducing luminescent molecule 24BD and halogenated benzene DITF and TITF, which exhibit reversible acid–base stimulus-responsive RTP properties. After detailed analysis of the crystal stacking structure, intermolecular interactions, and theoretical calculations, it was found that halogen bonds not only facilitate co-crystal formation, but also enhance SOC, thus promoting the ISC process and enabling RTP emission. Additionally, π–π interactions play a crucial role

in facilitating long-wavelength RTP emission. The different halogen bond strengths in the two co-crystals lead to varying degrees of protonation and deprotonation upon acid/base treatment, which results in distinct reversibility in their luminescent responses. This study revealed the causes of acid–base stimulus-responsive orange-red RTP in detail, which laid a foundation for the rational design of long-wavelength RTP materials. Moreover, the tunable phosphorescence lifetime, emission color and intensity in response to external stimuli may open new avenues for applying RTP co-crystals in sensing, information encryption, anti-counterfeiting security and other advanced functional materials.

Author contributions

Yuxuan Song: conceptualization, data curation, formal analysis, investigation, validation, visualization, and writing – original draft. Xingjia Jiang: data curation, formal analysis, and investigation. Guocui Pan: formal analysis. Bin Xu: funding acquisition, resources, and supervision. Wenjing Tian: funding acquisition, resources, supervision, and writing – review and editing.

Conflicts of interest

There are no conflicts to declare.

Data availability

All data supporting the findings of this study are available within the paper and its supplementary information (SI). Supplementary information: It mainly contains supplementary methods, supplementary figures S1–S25 and supplementary tables S1–S5. See DOI: **https://doi.org/10.1039/d5qm00717h**.

CCDC 2243007 contains the supplementary crystallographic data for this paper.[51]

Acknowledgements

This work was supported by the National Natural Science Foundation of China (22275065 and 52073116) and the Natural Science Foundation of Jilin Province (20240101003JJ).

Notes and references

1 Kenry, C. J. Chen and B. Liu, Enhancing the performance of pure organic room-temperature phosphorescent luminophores, *Nat. Commun.*, 2019, **10**, 2111.
2 Z. H. He, H. Q. Gao, S. T. Zhang, S. Y. Zheng, Y. Z. Wang, Z. H. Zhao, D. Ding, B. Yang, Y. M. Zhang and W. Z. Yuan, Achieving persistent, efficient, and robust room-temperature phosphorescence from pure organics for versatile applications, *Adv. Mater.*, 2019, **31**, 1807222.
3 S. Guo, W. B. Dai, X. Q. Chen, Y. X. Lei, J. B. Shi, B. Tong, Z. X. Cai and Y. P. Dong, Recent progress in pure organic room temperature phosphorescence of small molecular host-guest systems, *ACS Mater. Lett.*, 2021, **3**, 379–397.
4 Y. S. Wang, H. Q. Gao, J. Yang, M. M. Fang, D. Ding, B. Z. Tang and Z. Li, High performance of simple organic phosphorescence host-guest materials and their application in time-resolved bioimaging, *Adv. Mater.*, 2021, **33**, 2007811.
5 Z. Qian, C. L. Yang and Y. L. Zhao, Dynamic organic room-temperature phosphorescent systems, *Chemistry*, 2023, **9**, 2446–2480.
6 Y. H. Zhang, H. R. Li, M. D. Yang, W. B. Dai, J. B. Shi, B. Tong, Z. X. Cai, Z. Y. Wang, Y. P. Dong and X. Q. Yu, Organic room-temperature phosphorescence materials for bioimaging, *Chem. Commun.*, 2023, **59**, 5329–5342.
7 D. M. Guo, W. Wang, K. M. Zhang, J. Z. Chen, Y. Y. Wang, T. Y. Wang, W. M. Hou, Z. Zhang, H. H. Huang, Z. G. Chi and Z. Y. Yang, Visible-light-excited robust room-temperature phosphorescence of dimeric single-component luminophores in the amorphous state, *Nat. Commun.*, 2024, **15**, 3598.
8 X. Y. Dou, X. Wang, X. L. Xie, J. Zhang, Y. Li and B. Tang, Advances in polymer-based organic room-temperature phosphorescence materials, *Adv. Funct. Mater.*, 2024, **34**, 2314069.
9 J. M. Zhang, Z. H. Meng, Y. G. Zhen, P. He, P. P. Yu and W. P. Hu, Halogenated thienoacene derivatives with improved emission properties, *Chem. Res. Chin. Univ.*, 2024, **40**, 699–703.
10 P. C. Xue, P. P. Wang, P. Chen, J. P. Ding and R. Lu, Enhanced room-temperature phosphorescence of triphenylphosphine derivatives without metal and heavy atoms in their crystal phase, *RSC Adv.*, 2016, **6**, 51683–51686.
11 J. Yang, X. Zhen, B. Wang, X. M. Gao, Z. C. Ren, J. Q. Wang, Y. J. Xie, J. R. Li, Q. Peng, K. Y. Pu and Z. Li, The influence of the molecular packing on the room temperature phosphorescence of purely organic luminogens, *Nat. Commun.*, 2018, **9**, 840.
12 J. Yuan, S. Wang, Y. Ji, R. F. Chen, Q. Zhu, Y. R. Wang, C. Zheng, Y. Tao, Q. L. Fan and W. Huang, Invoking ultralong room temperature phosphorescence of purely organic compounds through H-aggregation engineering, *Mater. Horiz.*, 2019, **6**, 1259–1264.
13 M. Y. He, T. Tan, H. Hou, F. L. Guo, X. J. Wang, Q. K. Li, L. J. Qu, K. T. Wang, Y. B. Li and C. L. Yang, Construction of cross-linked polymer phosphorescence by functionalization of cyclotriphosphazene, *Adv. Opt. Mater.*, 2025, **13**, 2403164.
14 F. L. Ma, B. Wu, S. W. Zhang, J. H. Jiang, J. H. Shi, Z. Y. Ding, Y. Zhang, H. Z. Tan, P. Alam, J. W. Y. Lam, Y. Xiong, Z. Li, B. Z. Tang and Z. Zhao, Lone pairs-mediated multiple through-space interactions for efficient room-temperature phosphorescence, *J. Am. Chem. Soc.*, 2025, **147**, 10803–10814.
15 Y. Liu, G. Zhan, Z. W. Liu, Z. Q. Bian and C. H. Huang, Room-temperature phosphorescence from purely organic materials, *Chin. Chem. Lett.*, 2016, **27**, 1231–1240.

16 J. G. Wang, X. G. Gu, H. L. Ma, Q. Peng, X. B. Huang, X. Y. Zheng, S. H. P. Sung, G. G. Shan, J. W. Y. Lam, Z. G. Shuai and B. Z. Tang, A facile strategy for realizing room temperature phosphorescence and single molecule white light emission, *Nat. Commun.*, 2018, **9**, 2963.
17 Y. X. He, J. Wang, Q. Y. Li, S. L. Qu, C. F. Zhou, C. Z. Yin, H. L. Ma, H. F. Shi, Z. G. Meng and Z. F. An, Highly efficient room-temperature phosphorescence promoted via intramolecular-space heavy-atom effect, *Adv. Opt. Mater.*, 2023, **11**, 2201641.
18 Y. Han, M. Li, J. W. Lai, W. T. Li, Y. J. Liu, L. Q. Yin, L. Q. Yang, X. G. Xue, R. Vajtai, P. M. Ajayan and L. Wang, Rational design of oxygen-enriched carbon dots with efficient room-temperature phosphorescent properties and high-tech security protection application, *ACS Sustainable Chem. Eng.*, 2019, **7**, 19918–19924.
19 H. D. Sun, Z. L. Xie, H. L. Wang, Y. Z. Wu, B. B. Du, C. Guan and T. Yu, Manipulating room-temperature phosphorescence *via* lone-pair electrons and empty-orbital arrangements and hydrogen bond adjustment, *J. Mater. Chem. C*, 2022, **10**, 8854–8859.
20 W. Z. Yuan, X. Y. Shen, H. Zhao, J. W. Y. Lam, L. Taa, P. Lu, C. L. Wang, Y. Liu, Z. M. Wang, Q. Zheng, J. Z. Sun, Y. G. Ma and B. Z. Tang, Crystallization-induced phosphorescence of pure organic luminogens at room temperature, *J. Phys. Chem. C*, 2010, **114**, 6090–6099.
21 Y. Gong, G. Chen, Q. Peng, W. Z. Yuan, Y. J. Xie, S. H. Li, Y. M. Zhang and B. Z. Tang, Achieving persistent room temperature phosphorescence and remarkable mechanochromism from pure organic luminogens, *Adv. Mater.*, 2015, **27**, 6195–6201.
22 B. Zhou and D. P. Yan, Hydrogen-bonded two-component ionic crystals showing enhanced long-lived room-temperature phosphorescence via TADF-assisted Förster resonance energy transfer, *Adv. Funct. Mater.*, 2019, **29**, 1807599.
23 E. Hamzehpoor and D. F. Perepichka, Crystal engineering of room temperature phosphorescence in organic solids, *Angew. Chem., Int. Ed.*, 2020, **59**, 9977–9981.
24 Y. Zheng, Z. H. Wang, J. W. Liu, Y. F. Zhang, L. Gao, C. Wang, X. Zheng, Q. Zhou, Y. Yang, Y. B. Li, H. L. Tang, L. J. Qu, Y. L. Zhao and C. L. Yang, Long-lived room temperature phosphorescence crystals with green light excitation, *ACS Appl. Mater. Interfaces*, 2022, **14**, 15706–15715.
25 A. Huang, Y. Y. Fan, K. Wang, Z. Z. Wang, X. Y. Wang, K. Chang, Y. Gao, M. Z. Chen, Q. Q. Li and Z. Li, Organic persistent RTP crystals: from brittle to flexible by tunable self-partitioned molecular packing, *Adv. Mater.*, 2023, **35**, 2209166.
26 Z. C. Pan, J. M. Song, S. S. Zhang, P. Zeng, J. Mei and D. H. Qu, Tailoring raloxifene into single-component molecular crystals possessing multilevel stimuli-responsive room-temperature phosphorescence, *Sci. Bull.*, 2024, **69**, 1237–1248.
27 B. B. Ding, L. W. Ma, Z. Z. Huang, X. Ma and H. Tian, Engendering persistent organic room temperature phosphorescence by trace ingredient incorporation, *Sci. Adv.*, 2021, **7**, eabf9668.
28 Y. S. Wang, M. X. Gao, J. Ren, J. Y. Liang, Y. Zhao, M. M. Fang, J. Yang and Z. Li, Exciplex-induced TADF, persistent RTP and ML in a host-guest doping system, *Mater. Chem. Front.*, 2023, **7**, 1093–1099.
29 A. W. K. Law, T. S. Cheung, J. Y. Zhang, N. L. C. Leung, R. T. K. Kwok, Z. Zhao, H. H. Y. Sung, I. D. Williams, Z. J. Qiu, P. Alam, J. W. Y. Lam and B. Z. Tang, Sergeant-and-soldier effect in an organic room-temperature phosphorescent host-guest system, *Adv. Mater.*, 2024, **36**, 2410739.
30 X. X. Jiao, W. L. Zhang, J. R. Zhi, Y. X. Wang, M. Y. Wang, Z. Y. Liu and J. P. Li, Ultra-long organic RTP host-guest doped systems based on pure 4-(1H-imidazole-1-yl)methyl benzoate as versatile hosts, *Mater. Chem. Front.*, 2025, **9**, 1166–1173.
31 Y. Zhao, X. G. Yang, X. M. Lu, C. D. Yang, N. N. Fan, Z. T. Yang, L. Y. Wang and L. F. Ma, {Zn6} cluster based metal-organic framework with enhanced room-temperature phosphorescence and optoelectronic performances, *Inorg. Chem.*, 2019, **58**, 6215–6221.
32 X. G. Yang, Z. M. Zhai, X. M. Lu, J. H. Qin, F. F. Li and L. F. Ma, Hexanuclear Zn(II)-induced dense π-stacking in a metal-organic framework featuring long-lasting room temperature phosphorescence, *Inorg. Chem.*, 2020, **59**, 10395–10399.
33 M. Gutiérrez, C. Martín, J. Hofkens and J. C. Tan, Long-lived highly emissive MOFs as potential candidates for multi-photonic applications, *J. Mater. Chem. C*, 2021, **9**, 15463–15469.
34 Y. F. Cao, K. M. Zhang, H. Y. Wang, S. Y. Jiang, F. Lin, D. M. Guo, Y. C. Li, H. H. Huang, Z. Y. Yang and Z. G. Chi, Deep-red ultralong room temperature phosphorescence of chitosan-based nanofibrous membrane activated by carboxylic acids, *Chem. Eng. J.*, 2023, **476**, 146781.
35 S. T. Li, Y. W. Qi, A. Li, Y. Q. Yang, M. D. Shan, K. Yang, Y. Wang and Z. Li, A new strategy to enhance room temperature phosphorescence performance in physical doping polymer system, *Adv. Optical Mater.*, 2025, **13**, 2402201.
36 R. Tian, S. M. Xu, Q. Xu and C. Lu, Large-scale preparation for efficient polymer-based room-temperature phosphorescence *via* click chemistry, *Sci. Adv.*, 2020, **6**, eaaz6107.
37 S. D. Xiong, Y. Xiong, D. L. Wang, Y. W. Pan, K. Y. Chen, Z. Zhao, D. Wang and B. Z. Tang, Achieving tunable organic afterglow and UV-irradiation-responsive ultralong room-temperature phosphorescence from pyridine-substituted triphenylamine derivatives, *Adv. Mater.*, 2023, **35**, 2301874.
38 N. Y. Li, X. P. Yang, B. B. Wang, P. Y. Chen, Y. X. Ma, Q. Q. Zhang, Y. Y. Huang, Y. Zhang and S. Y. Lü, Color-tunable room-temperature phosphorescence from non-aromatic-polymer-involved charge transfer, *Adv. Sci.*, 2024, **11**, 2404698.
39 Z. Y. Zhang, Y. Chen and Y. Liu, Efficient room-temperature phosphorescence of a solid-state supramolecule enhanced by cucurbit[6]uril, *Angew. Chem., Int. Ed.*, 2019, **58**, 6028–6032.

40 J. Wang, Z. Z. Huang, X. Ma and H. Tian, Visible-light-excited room-temperature phosphorescence in water by cucurbit[8]uril-mediated supramolecular assembly, *Angew. Chem., Int. Ed.*, 2020, **59**, 9928–9933.
41 H. Zheng, Z. Y. Zhang, S. Z. Cai, Z. F. An and W. Huang, Enhancing purely organic room temperature phosphorescence via supramolecular self-assembly, *Adv. Mater.*, 2024, **36**, 2311922.
42 C. F. Feng, S. Li, X. X. Xiao, Y. L. Lei, H. Geng, Y. Liao, Q. Liao, J. N. Yao, Y. S. Wu and H. B. Fu, Excited-state modulation for controlling fluorescence and phosphorescence pathways toward white-light emission, *Adv. Opt. Mater.*, 2019, **7**, 1900767.
43 K. Liu, S. Li, L. Y. Fu, Y. L. Lei, Q. Liao and H. B. Fu, Cocrystallization tailoring radiative decay pathways for thermally activated delayed fluorescence and room-temperature phosphorescence emission, *Nanoscale*, 2022, **14**, 6305–6311.
44 X. Wang, Z. R. Wang, X. Wang, F. Y. Kang, Q. F. Gu and Q. C. Zhang, Recent advances of organic cocrystals in emerging cutting-edge properties and applications, *Angew. Chem., Int. Ed.*, 2024, **63**, e202416181.
45 A. Abe, K. Goushi, M. Mamada and C. Adachi, Organic binary and ternary cocrystal engineering based on halogen bonding aimed at room-temperature phosphorescence, *Adv. Mater.*, 2024, **36**, 2211160.
46 C. C. Zhang, X. J. Jiang, C. Wang, Z. Y. Liu, B. Xu and W. J. Tian, Organic room temperature phosphorescence co-crystal with reversible acid/base stimulus response, *Smart Mol.*, 2025, e20240054.
47 C. F. Yang, S. Y. Fu, S. Z. Li, F. Li, Y. Su, T. T. Li, H. P. Liu, X. T. Zhang and W. P. Hu, A chiral cocrystal strategy producing room-temperature phosphorescence and enhancing circularly polarized luminescence, *Adv. Opt. Mater.*, 2025, **13**, 2402522.
48 L. F. Bian, H. F. Shi, X. Wang, K. Ling, H. L. Ma, M. P. Li, Z. C. Cheng, C. Q. Ma, S. Z. Cai, Q. Wu, N. Gan, X. F. Xu, Z. F. An and W. Huang, Simultaneously enhancing efficiency and lifetime of ultralong organic phosphorescence materials by molecular self-assembly, *J. Am. Chem. Soc.*, 2018, **140**, 10734–10739.
49 S. L. Qu, K. Shen, B. S. Wu, Y. X. He, Z. Zhao, C. Z. Yin, Z. F. An, S. M. Yan and H. F. Shi, Regulating phosphorescence lifetime of organic cocrystals by alkyl engineering, *Cryst. Growth Des.*, 2023, **23**, 31–36.
50 Y. B. Peng, G. X. Zhou, R. Y. Zhang, L. Wang, Y. Z. Ma, G. Peng and X. M. Ren, Chiral cocrystals with circularly polarized persistent phosphorescence and large second harmonic generation, *Surf. Interfaces*, 2025, **61**, 106114.
51 CCDC 2243007: Experimental Crystal Structure Determination, 2025, DOI: **10.5517/ccdc.csd.cc2f912w**.